Chemistry–A European Journal
Full Paper
doi.org/10.1002/chem.202000547
Chemistry Europe
European Chemical Societies Publishing

Graphene

Poly(methyl methacrylate)-Assisted Exfoliation of Graphite and Its Use in Acrylonitrile-Butadiene-Styrene Composites

Silvia Gentiluomo,[a, b] Sanjay B. Thorat,*[c] Antonio Esau Del Río Castillo,[a] Peter S. Toth,[a, d] Jaya Kumar Panda,[a] Vittorio Pellegrini,[a, c] and Francesco Bonaccorso*[a, c]

Abstract: One of the applications of graphene in which its scalable production is of utmost importance is the development of polymer composites. Among the techniques used to produce graphene flakes, the liquid-phase exfoliation (LPE) of graphite stands out due to its versatility and scalability. However, solvents suitable for the LPE process are generally toxic and have a high boiling point, making the processing challenging. The use of low boiling point solvents could be convenient for the processing, due to the easiness of their removal. In this study, the use of poly(methyl methacrylate) (PMMA) as a stabilizing agent is proposed for the production of graphene flakes in a low boiling point solvent, that is, acetone. The graphene dispersions produced in the mixture acetone-PMMA have higher concentration, +175%, and contain a higher percentage of few-layer graphene flakes (<5 layers), that is, +60%, compared to the dispersions prepared in acetone. The as-produced graphene dispersions are used to develop graphene/acrylonitrile-butadiene-styrene composites. The mechanical properties of the pristine polymer are improved, that is, +22% in the Young's modulus, by adding 0.01 wt.% of graphene flakes. Moreover, a decrease of ≈20% in the oxygen permeability is obtained by using 0.1 wt.% of graphene flakes filler, compared to the unloaded matrix.

Introduction

Graphene is a two-dimensional material with potential applications in various fields, for example, electronics,[1–7] optoelectronics,[8–10] energy[11–13] and polymer composites.[14–19] The large scale production of graphene, as well as other 2D materials,[20] is still an open issue, both at the academic and particularly at the industrial level, to guarantee its promising for the aforementioned applications.[20,21] Graphene can be produced by both bottom-up and top-down approaches.[22,23] In the first case, the atom-by-atom assembling of the graphene honeycomb lattice is carried out through techniques as the chemical vapour deposition (CVD),[24–27] and growth on SiC.[28–32] The top-down approach, instead, consists in peeling-off the layers of graphite,[22,23] by exploiting methods as the micromechanical cleavage (MC)[33,34] and the liquid-phase exfoliation (LPE).[23,35–42] The LPE process of graphite fulfils the industrial scale demand of graphene for the production of inks and the development of graphene-based polymer composites, due to its scalability.[20,21]

A key requirement for the LPE process relies on the minimization of the interfacial tension between the solvent and the exfoliated flakes.[43–45] This means, in the case of graphite, that the solvents should have a surface tension (γ) of about 40 $m_N m^{-1}$.[35] Following this requirement, *N*-methyl-2-pyrrolidone (NMP, $\gamma = 40.21$ $m_N m^{-1}$)[46] and γ-butyrolactone (GBL, $\gamma =$ 46.5 $m_N m^{-1}$)[46] can be considered, for example, suitable solvents for the exfoliation of graphite.[35] However, the solvents that are generally used for the exfoliation of graphite are mostly toxic (NMP has been reported to be teratogenic,[47] GBL causes severe respiratory problems[48]), and have a high boiling point (boiling point $T_b \geq 200\,^{\circ}C$).[49] High boiling point solvents suffer several issues also from the technical point of view for their exploitation in different applications, such as coatings and polymer composites.[50–52] In particular, for the latter application, high boiling point solvents are difficult to remove during the processing. In fact, the presence of trapped solvent causes the formation of voids,[53,54] compromising the performances of the composite, for example, mechanical, electrical and thermal properties.[53,54]

[a] S. Gentiluomo, Dr. A. E. Del Río Castillo, Dr. P. S. Toth, Dr. J. K. Panda, Dr. V. Pellegrini, Dr. F. Bonaccorso
Graphene Labs, Instituto Italiano di Tecnologia
Via Morego 30, Genoa, 16163 (Italy)
E-mail: francesco.bonaccorso@iit.it

[b] S. Gentiluomo
Dipartimento di Chimica e Chimica Industriale, Università di Genova
Via Dodecaneso 31, Genoa, 16146 (Italy)

[c] Dr. S. B. Thorat, Dr. V. Pellegrini, Dr. F. Bonaccorso
BeDimensional SpA
Via Albisola 121, Genoa, 16163 (Italy)
E-mail: s.thorat@bedimensional.it

[d] Dr. P. S. Toth
Department of Physical Chemistry & Material Science
University of Szeged
Rerrich Sq 1, 6720 Szeged (Hungary)

Supporting information and the ORCID identification number(s) for the author(s) of this article can be found under: https://doi.org/10.1002/chem.202000547.

Part of a Special Issue focusing on the "Chemical Functionalization of 2D Materials", which supports the symposium on the topic held at the E-MRS 2020 Spring Meeting. To view the complete issue, visit Issue 29.

In an ideal scenario, the production and the processing of graphene should be performed by using low boiling point solvents. Solvents possessing a boiling point lower than about 90 °C are desirable, in order to avoid side effects in the development of graphene-based polymer composites, for example, incipient degradation and shrinkage of the polymer matrix.[55,56] Moreover, an easy removal of the solvent is preferable, as the solvent residues affect the physical and chemical properties of the composite material.[57,58] Low boiling point solvents could also facilitate the use of the graphene dispersions in printing methods as inkjet printing,[20,59,60] flexography[61] or spray coating.[62] In this regard, low boiling point solvents, such as isopropanol (IPA) ($T_b \approx 82$ °C[49]) and ethanol ($T_b \approx 78$ °C[49]), have limitations for polymer composites production, due to the fact that they are able to dissolve just a few polymers, for example, polyvinyl butyral (PVB),[63] ethyl cellulose (EC)[64] and polyvinyl pyrrolidone (PVP).[65] Among the low boiling point solvents, acetone stands out because it is harmless,[66] and has the capability to dissolve many polymers, for example, cellulose acetate (CA),[67] acrylonitrile butadiene styrene (ABS),[68] poly(methyl methacrylate) (PMMA),[69,70] styrene-acrylonitrile,[71] poly(ethylene oxide)[72] and poly(vinyl acetate),[73,74] just to cite a few.

Nevertheless, the aforementioned low boiling point solvents do not fulfil the requirement of minimizing the free Gibbs energy for the exfoliation of graphite,[46] for example, $\gamma_{acetone} = 26.67\ mN\ m^{-1}$.[75] As a matter of fact, the LPE process carried out in low boiling point solvents has been demonstrated to achieve lower exfoliation yield by weight, that is, the ratio between the weight of the final graphitic material and the one of the starting graphite flakes,[22,23] compared to the exfoliation carried out in high boiling point solvents.[60,76] For example, O'Neill et al.[76] compared the exfoliation of graphite in IPA and NMP processed in the same conditions, in terms of concentration (C_g), obtaining $C_{g\text{-}IPA} \approx 50\ mg\ L^{-1}$ in IPA and $C_{g\text{-}NMP} \approx 200\ mg\ L^{-1}$ in NMP.

In general, the stabilization of exfoliated graphene flakes in low boiling point solvents is assisted by using polymers through steric stabilization.[64,65,77,78] The polymeric aliphatic chains bind to the basal plane of graphene, either covalently or through van der Waals forces.[77] Consequently, repulsive forces are present between the polymer chains, hindering the restacking of the flakes during and after the exfoliation process.[77] For example, PMMA, which is an inexpensive (≈€150 per ton[79]) and nontoxic polymer,[80] forms π–π bonds between the carbonyl groups and the graphene, promoting the attachment of the polymer chains onto the graphene flakes.[81–83] Moreover, PMMA is able to form homogeneous blends with other polymers, for example, polyvinyl chloride (PVC),[84] polyaniline (PANI),[85] polyethylene glycol (PEG),[86] ABS[87] among others. The polymer miscibility of PMMA can be exploited to obtain a homogenous distribution of the graphene flakes into the polymeric matrix.

In this work, we demonstrate the LPE of graphite using acetone as the solvent and PMMA as the stabilizing agent. The as-produced graphene-based dispersions in the acetone-PMMA mixture are characterized by increased concentration, that is, +175%, and contain a higher percentage of few-layer graphene (FLG) flakes (<5 layers), that is, +60%, compared to the dispersions prepared in acetone.

The FLG dispersions produced using acetone–PMMA are tested as fillers in ABS composites, measuring their performance in gas barrier membranes. The graphene-PMMA/ABS composites (0.01 wt.% of FLG flakes) show an improvement of ≈22% and ≈17% in the Young's modulus and tensile strength, respectively, compared to the bare ABS. Furthermore, the oxygen permeability (OP) is reduced by approximately 20% in the composites with 0.1 wt.% of FLG flakes loading compared to the unfilled ABS.

Results and Discussion

Characterization of the exfoliated graphite dispersions

The graphite exfoliation is carried out in pure acetone and acetone with 1%wt. PMMA. The obtained dispersions are both further processed at three different centrifugal accelerations: 200, 4300 and 17000 *g*.

The two dispersions are analyzed through Raman spectroscopy, in order to obtain an indication concerning the flake thickness, to give an information regarding a possible doping effect and to identify the type of defects.[88–90] The Raman spectrum of graphene presents the characteristic G, D and the 2D peaks, more information regarding the origin of these features are reported in the Supporting Information.[88,89]

Among the features of the Raman spectrum of graphene, the 2D peak is composed by various components in few-layer graphene (FLG) and multi-layer graphene (MLG), in which the main components are $2D_1$ and $2D_2$.[88] In graphite, the intensity of the component $2D_1$ [$I(2D_1)$], is roughly half of the intensity of the component $2D_2$ [$I(2D_2)$].[88,89] During the exfoliation process, the $I(2D_1)$ increases and the $I(2D_2)$ decreases, due to a reduction of the thickness of the flakes.[88]

Figure 1a represents the Raman spectra for the dispersions FLG (blue line) and FLG-PMMA (red line) obtained using a centrifugal acceleration of 17000 *g*. The spectra of graphite (black line) and PMMA (green line) are also plotted for comparison.

All the spectra, except the bare PMMA, are normalized to the graphitic G peak. The normalized intensity ratios $I(2D_1)/I(G)$ expressed as function of $I(2D_2)/I(G)$ gives an insight of the thickness of the flakes.[20] In fact, the points on the dashed line in Figure 1b–d are considered as multi-layer flakes (MLG) [$I(2D_1)/I(G) = I(2D_2)/I(G)$], while the points below the line [$I(2D_1)/I(G) < I(2D_2)/I(G)$] are considered as graphitic flakes.[20,88,91] The flakes with 5 layers or less, for example, FLG, are represented by points located above the few-layers condition $I(2D_1)/I(G) > I(2D_2)/I(G)$.[20,88,91] In this study, the percentage of the points satisfying the FLG condition over the total number of points are approximately 36, 53 and 93% for the dispersions in acetone and about 58, 70 and 98% for the ones in acetone-1 wt.% PMMA, centrifuged at 200, 4300 and 17000 *g*, respectively. Therefore, the dispersions in acetone and acetone-1 wt.% PMMA will be called "FLG" and "FLG-PMMA", respectively. The reduction in the number of layers of the flakes leads to a drop

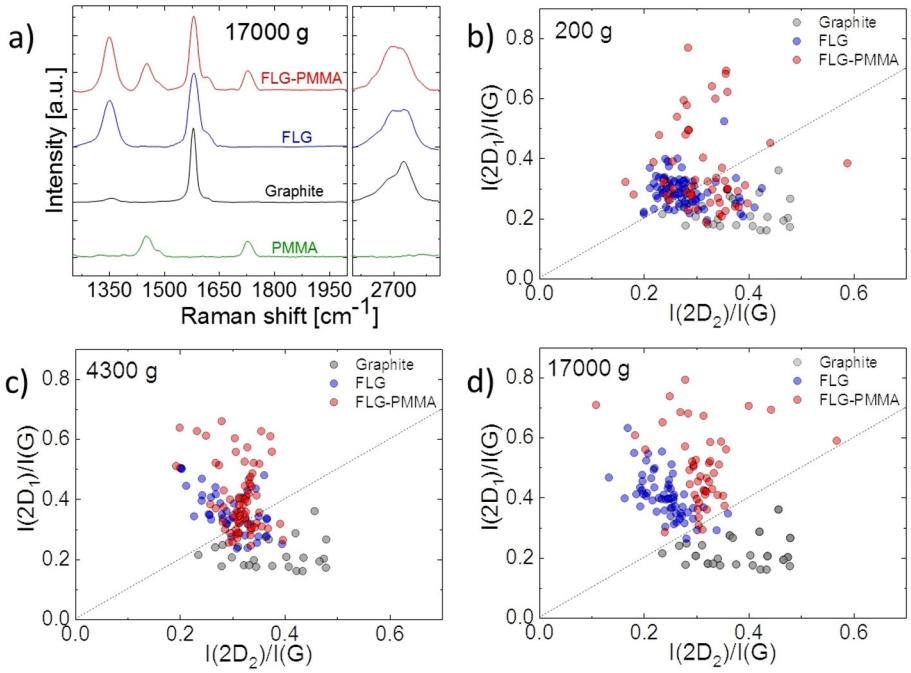

Figure 1. (a) Raman spectra of the dispersions FLG PMMA (red) and FLG (blue) obtained with a centrifugal acceleration of 17 000 *g*, graphite (black) and bare PMMA (green). The normalized intensities $I(2D_2)/I(G)$ vs. $I(2D_1)/I(G)$ shows the distribution of FLG and graphitic flakes for the dispersions FLG and FLG-PMMA obtained with centrifugal accelerations (b) 200 *g*, (c) 4300 *g* and (d) 17 000 *g*.

of the $I(2D_2)/I(2D_1)$ ratio, as the intensity of the component $2D_1$ increases,[88] (see Figure S1). Thus, the FLG-PMMA dispersions present a higher percentage of FLG flakes compared to the FLG dispersions. In addition, as reported above, the processing conditions clearly influence the morphology (i.e., lateral size and thickness) of the flakes in both dispersions. In fact, the percentage of FLG flakes in both dispersions increases with the centrifugal acceleration (see Figure 1 b–d), although the percentage of FLG flakes is higher in the one containing PMMA.

The presence of defects on the basal plane, for example, vacancies,[92] damage the properties of graphene, for example, decrease in the Young's modulus.[93,94] Thus, in order to distinguish between edge defects with the basal plane ones, we considered the correlation between the FWHM(G) and the ratio of the intensities and the area of the D peak and the G peak, that is, I(D)/I(G) and A(D)/A(G). In fact, a linear correlation between the FWHM(G) and I(D)/I(G), as well as with A(D)/A(G) indicates that the defects are located on the basal plane rather than on the edges.[95] In Figure S2, the I(D)/I(G) and A(D)/A(G) versus the FWHM(G) of the dispersions show no correlation. Therefore, the defects are mainly due to flake edges.[95]

The PMMA is supposed to hinder the re-stacking of the exfoliated graphite flakes during and after the exfoliation process, by binding with graphene through π–π interactions with the carbonyl groups (C=O),[82,83,96] providing repulsive forces among the flakes.[97] The results of Raman spectroscopy indicate that the PMMA does not cause a doping effect (Figure S3), so that the possible interaction between graphene and PMMA is not influencing the electrical properties of graphene.

The thickness of the as-produced flakes are also analyzed by atomic force microscopy (AFM). Considering substrate effects, solvent and polymer residuals, the thickness of the FLG flakes (measured with AFM in tapping mode) is, on average, lower than 4 nm.[98–101] Therefore, the flakes having a thickness <4 nm will be referred as exfoliated flakes. The number of exfoliated flakes is calculated as a percentage over the thickness of 100 flakes measured with the AFM.

Representative AFM images of the exfoliated flakes are shown in Figure 2 a,b and Figure S4 a–d, reporting the thickness statistics in the insets. Nevertheless, the presence of PMMA residue in the samples (demonstrated by thermogravimetric analysis, TGA, Figure S5), overestimates the flake thickness. The percentages of exfoliated flakes are 13, 35 and 53% for the FLG dispersions, and 30, 42 and 88% for the FLG-PMMA dispersions, centrifuged at 200, 4300 and 17 000 *g*, respectively. The FLG-PMMA dispersion contains a higher percentage of exfoliated flakes compared to the FLG one, for all the three centrifugal accelerations, in agreement with the Raman data.

The lateral sizes of the exfoliated flakes are evaluated using TEM. Representative TEM images of the exfoliated graphite flakes are shown in Figure 2 c,d and Figure S6 a–d with their corresponding lateral size statistics reported in the insets. The statistical analysis of the TEM images indicates that the lateral sizes of the flakes are: 520 nm (log normal S.D. 0.57), 400 nm (log normal S.D. 0.50), 300 nm (log normal S.D. 0.60) for the FLG dispersions, and 600 nm (log normal S.D. 0.40), 370 nm (log normal S.D. 0.43), 270 nm (log normal S.D. 0.33) for the FLG-PMMA dispersions, centrifuged at 200, 4300 and 17 000 *g*, respectively.

These data indicate that the distribution of the lateral size of the flakes is more homogeneous, for example, log normal S.D.

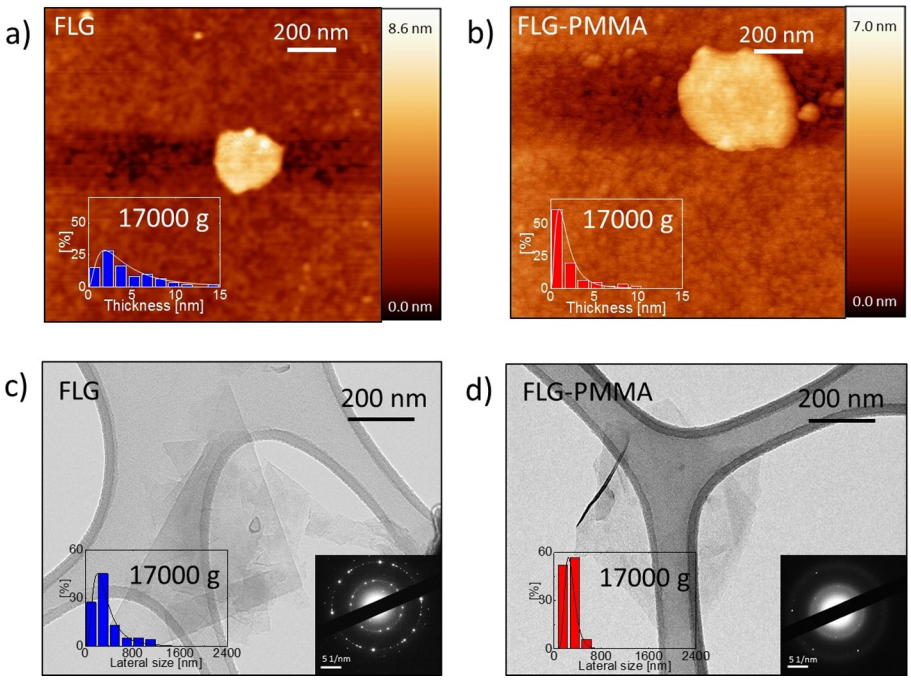

Figure 2. AFM images of exfoliated graphite flakes in the dispersions a) FLG and b) FLG-PMMA centrifuged at 17 000 *g*. The thickness distribution is given as inset. TEM images of exfoliated graphite flakes in the dispersions c) FLG and d) FLG-PMMA centrifuged at 17 000 *g*. The lateral size distribution and the SAED patterns are given as insets.

0.40 for the FLG-PMMA dispersion at 200 *g*, than in the flakes of the FLG dispersion, that is, log normal S.D. 0.57 for 200 *g*. The lateral size distributions of the FLG and FLG-PMMA dispersions are represented through the intervals of confidence in Figure S7. The selected area electron diffraction (SAED) pattern is presented in the insets of Figure 2 c,d, showing the typical 6-fold pattern of graphene,[102–104] demonstrating that the crystalline structure of the flakes has not been damaged during the exfoliation process.

The concentration is measured through vacuum filtration (see "Vacuum filtration" section in the Experimental Section). The concentrations obtained in the exfoliated graphite dispersions are $80 \pm 20\ mg\,L^{-1}$, $30 \pm 10\ mg\,L^{-1}$ and $1 \pm 0.2\ mg\,L^{-1}$ for the FLG dispersions, and $220 \pm 40\ mg\,L^{-1}$, $90 \pm 20\ mg\,L^{-1}$ and $30 \pm 6\ mg\,L^{-1}$ for the dispersions FLG-PMMA, centrifuged at 200, 4300 and 17 000 *g*, respectively. It can be noticed that the concentration of the FLG-PMMA dispersions is higher compared to the FLG dispersion, that is, there is an improvement of +175, +200 and +2900%. To assess that the presence of PMMA is not affecting the concentration measurements, we carried out TGA (see the Experimental Section). The residual of the TGA gives information regarding the mass of FLG in the dispersion (check the Supporting Information). The measured mass of the exfoliated graphite is averaged from five TGA runs, resulting in the FLG mass for the FLG-PMMA dispersion centrifuged at 200 g of $227 \pm 8\ mg\,L^{-1}$ (Figure S9).

The measured mass of exfoliated graphite is in agreement with the previous results, for example, the mass of the exfoliated graphite is $227 \pm 8\ mg\,L^{-1}$ for the sample FLG-PMMA centrifuged at 200 *g* (Figure S8).

In order to calculate also the effective concentration of the FLG-PMMA dispersions, the extinction coefficient of the FLG-PMMA dispersion is evaluated using optical extinction spectroscopy (OES), considering the exfoliated graphite mass measured through the TGA. The estimated extinction coefficient is $0.04954 \pm 0.00135\ L\,mg^{-1}\,m^{-1}$. (Figure S10; see Experimental Section and Supporting Information). Therefore, the concentrations of the FLG-PMMA dispersions centrifuged at 4300 and 17 000 *g* obtained through OES are $74.6 \pm 0.1\ mg\,L^{-1}$ and $30.1 \pm 0.2\ mg\,L^{-1}$, respectively, in agreement with the concentration measurements obtained through vacuum filtration.

The obtained results, summarized in Table 1, highlight the fact that the FLG-PMMA dispersions contains thinner flakes and present a higher concentration compared to the FLG ones.

We propose that the difference in the morphology and concentration between the two dispersions is due to the presence of PMMA. Both acetone and the mixture of acetone-1 wt.% PMMA have a surface tension that do not match the surface energy of the flakes, being $23.8 \pm 0.4\ mN\,m^{-1}$ and $23.3 \pm 0.2\ mN\,m^{-1}$, respectively. The surface tension is measured through contact angle, for more information see the Experimental Section. Therefore, in the FLG-PMMA dispersions, the re-stacking of the flakes is hindered due the steric repulsion between the polymer chains, attached to the flakes.[77]

In order to explain the increase in the concentration of flakes in suspension associated to the presence of PMMA, the density (ρ) and the viscosity (η) of the mediums used for the exfoliation process are measured (Table 2). The results show that the presence of PMMA does not affect the ρ of the mixture, while the η is increased by 90%.

Table 1. Concentration, percentage of FLG and lateral size of the FLG and FLG-PMMA dispersions. The corresponding standard deviations for the concentration and lognormal standard deviation for the lateral size are reported in parentheses.

	FLG @200 *g*	FLG-PMMA	FLG @4300 *g*	FLG-PMMA	FLG @17 000 *g*	FLG-PMMA
C [mg L^{-1}]	80 (20)	220 (40)	30 (10)	90 (0.20)	1 (0.2)	30 (6)
FLG [%]	36	58	53	70	93	98
Lateral size [nm]	520 (0.57)	600 (0.40)	400 (0.50)	370 (0.43)	300 (0.60)	270 (0.33)

Table 2. ′
Density (ρ) and viscosity (η) of acetone and the mixture acetone-PMMA with the corresponding standard deviations in parenthesis.

	ρ [g cm^{-3}]	η [mPa s]
Acetone	0.80 (0.02)	0.295 (0.001)
Acetone-1 wt.% PMMA	0.77 (0.03)	0.559 (0.001)

The PMMA can affect also the sedimentation behavior of the exfoliated flakes during the purification step, carried out through sedimentation-based separation (SBS).[35,105]

The SBS technique is usually performed on particles dispersed in a solvent, applying a force field.[106,107] Among the forces acting during SBS, there is the centrifugal force $F_c = m_p \omega^2 r$, which is proportional to the mass of the particle (m_p), the distance from the rotational axes (r) and the square of the angular velocity (ω^2).[107] The buoyant force $F_b = -ms\ \omega^2\ r$, in which ms is the mass of the displaced solvent, and the frictional force $F_f = -f\sigma$, which depends on the friction coefficient between the solvent and the particle (f) and the sedimentation velocity of the particle itself (σ).[107] The sedimentation coefficient is defined as in Equation (1):[107,108]

$$S = \frac{\sigma}{\omega^2 r} = \frac{m_p\left(1 - \frac{\rho_s}{\rho_p}\right)}{f} \quad (1)$$

in which the ρ of the solvent and the particle are expressed as ρ_s and ρ_p, respectively. Thick and large flakes possess higher sedimentation coefficients compared to the small flakes, thus having a fast sedimentation.[107–109] It is possible to prepare dispersions containing flakes with different lateral size, by changing the parameters of the centrifugation.[108,110]

The sedimentation coefficient depends also on the features of the medium, as the density ρ_s and the viscosity η_s. The η_s is present in the friction coefficient, which can be obtained through Equation (2).

$$F = 6\pi\eta_s r \quad (2)$$

The sedimentation coefficient is inversely proportional to the η, so that the higher is the η of the solvent, the slower is the sedimentation of the particles.[107] Therefore, a higher quantity of flakes is retained in the supernatant in the FLG-PMMA dispersion compared to the FLG dispersions, after the centrifugation.

Moreover, the FLG percentage is increasing, while the concentration has a drop with the increase of the centrifugal acceleration. In fact, when the centrifugal acceleration is increased, the flakes are subjected to a higher centrifugal force, promoting the faster sedimentation of thicker flakes compared to the thinner flakes.[107] Hence, the concentration of the overall flakes and the population of thick flakes in the supernatant decrease, as the centrifugation acceleration passes from 200 to 17 000 *g*. A scheme of the observed phenomena is represented in Figure 3.

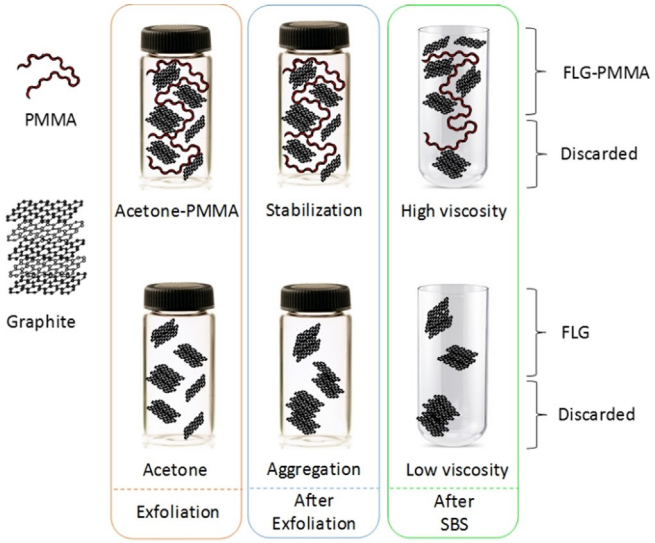

Figure 3. Scheme of the production of the FLG and FLG-PMMA dispersions: the graphite is dispersed in acetone and acetone-1 wt.% PMMA.

The results achieved by exfoliating graphite in acetone and PMMA indicate that the exfoliation yield (Y_w) has an improvement of 200%, in the same experimental conditions, that is, the same centrifugation speed. Table 3 presents the values of

Table 3. FoM of this study compared with other studies about exfoliation of graphite in acetone with the same centrifugal acceleration (4300 *g* for 30 min).

Reference	Solvent	Sonication time	Y_w [%]
[76]	Acetone	48 h	0.003
Our study	Acetone	6 h	0.003
Our study	Acetone-1 wt% PMMA	6 h	0.009

the FoM of this study compared with the work of O'Neill et al.[76]

Table S1 presents a comparison between our study and the other studies focused on the exfoliation of graphite in low boiling point solvents ($T_b < 90\,^{\circ}C$), using a polymer as a stabilizing agent.

Exfoliated graphite flakes as fillers in ABS composites

The ABS is a thermoplastic polymer which is used to improve the mechanical properties of polymer blends for the production of membranes for gas separation,[111–113] for example, CO_2.[113] The exfoliated flakes are used to improve both the mechanical and gas barrier properties of the pristine ABS.[114] Moreover, the ABS, or its component styrene acrylonitrile, is known to form miscible blends with PMMA.[87,115–119] The FLG and FLG-PMMA dispersions centrifuged at 200 g are chosen to prepare the composites. Although the chosen dispersions contain the lowest percentage of few-layer graphene flakes among the produced dispersions, the concentration obtained is the highest, that is, 220 mg mL^{-1} for the FLG-PMMA dispersion and 80 mg mL^{-1} for the FLG one.

FLG and FLG-PMMA as mechanical reinforcement in ABS composites

The mechanical properties of the composites are evaluated through tensile test. Two FoM are evaluated, that is, the Young's modulus, defined as the slope of the stress versus the strain curve in the elastic region,[120] and the tensile strength, defined as the highest value of stress reached during the testing.[120] In the literature, FLG[121] and graphene nanoplatelets (GnPs)[122–124] are used as fillers to improve the mechanical properties of ABS. Waheed et al.[121] produced ABS composites by using FLG and obtained improvements in the Young's modulus and the tensile strength of 71 and 43 %, compared to the unloaded ABS by using 0.24 vol % of loading, respectively. However, in the same study, both the Young's modulus and the tensile strength decrease, when the loading is >0.5 vol %, probably due to the agglomeration of the FLG flakes.[121] The ABS composites containing 8 wt. % GnPs in the studies of Du et al.[122,124] also present a drop in the tensile strength, that is, 10 %, compared to the pristine ABS, associated to the poor adhesion between the matrix and the filler. In our study, the Young's modulus and the tensile strength are enhanced by approximately 22 % and 17 %, respectively (Figure 4 a,b), compared to the pristine ABS, by using a FLG loading of 0.01 wt. %. The tensile strength value of the ABS-FLG-PMMA remains constant as the loading of FLG flakes is increased. On the contrary, there is no improvement of the tensile strength in the ABS-FLG composites compared to the unfilled polymer when the amount of filler is increased. These results indicate that the presence of PMMA in the ABS-FLG-PMMA composites may promote a homogeneous distribution of the FLG flakes into the polymeric matrix. Control samples ABS-PMMA are also tested for comparison purposes, to assess the impact of PMMA on the mechanical properties of the composite material. In this case, the Young's modulus and the tensile strength do not show any improvement compared to the pristine ABS (Figure S11 a,b).

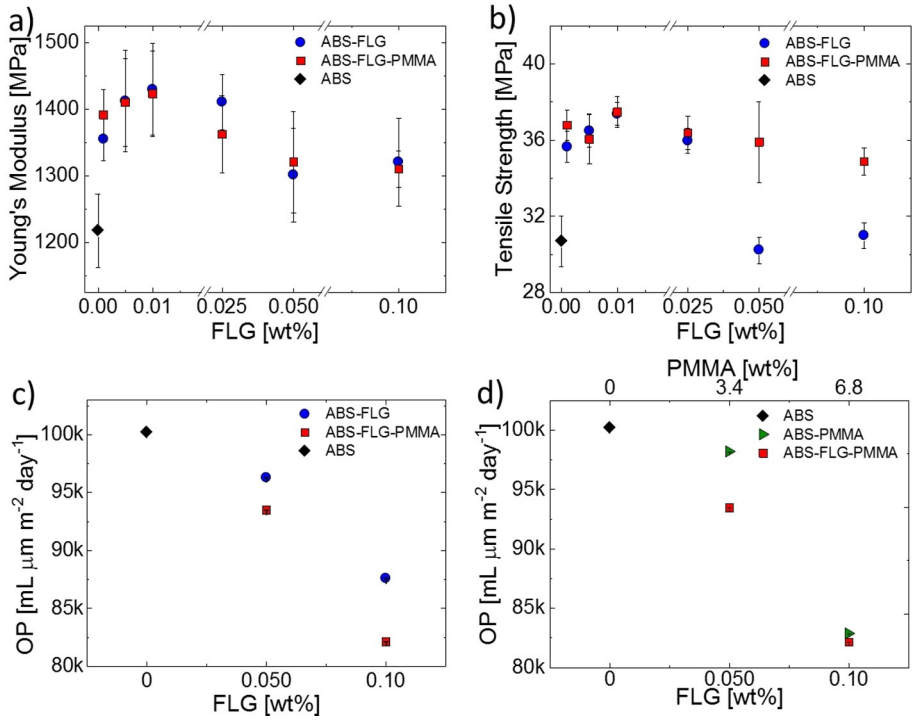

Figure 4. a) Young's modulus and b) tensile strength of the pristine ABS (black rhombuses), ABS-FLG (blue dots) and ABS-FLG-PMMA (red squares) composites with increasing loading of FLG; comparison of the OP of c) the pristine ABS vs. the composites ABS-FLG and ABS-FLG-PMMA and d) of the composites ABS-FLG-PMMA and of the ABS-PMMA samples (green triangles).

FLG and FLG-PMMA as fillers for gas barrier applications in ABS composites

The incorporation of the graphene flakes hinders the diffusion of gases through the polymer matrix, by forming a "maze-like" structure in the matrix.[125,126] In the literature, FLG flakes are used in the polymer composites to decrease the gas permeation.[127–129] In our study, the OP of the composites ABS-FLG and ABS-FLG-PMMA with a loading of 0.1 wt.% FLG is reduced by approximately 13% and 20%, respectively, compared to the pristine ABS (Figure 4c). In the composites ABS-FLG-PMMA, the OP is about 7% lower than in the ABS-FLG composites, as both PMMA and FLG may hinder the oxygen passage. To demonstrate that PMMA is playing a main role in the OP decrease in the ABS matrix, a control sample ABS-PMMA not containing FLG is tested. The ABS-PMMA sample containing 6.8 wt.% of PMMA presents an OP, which is about 17% lower compared to the pristine ABS. This data proves that also PMMA has an influence on the gas barrier properties in the composites ABS-FLG-PMMA (Figure 4d).

Conclusions

In this study, we exploited poly(methyl methacrylate) (PMMA) to aid the exfoliation of graphite in acetone. The presence of PMMA in dispersion prevents the re-stacking of the exfoliated flakes, improving their stabilization. In fact, the concentration of the dispersions increases from 80 mg L^{-1} to 220 mg L^{-1}, when PMMA is present for the samples prepared with a centrifugal acceleration of 200 *g*. Moreover, the percentage of few-layer graphene (FLG) flakes (<5 layers) is 60% higher in acetone-PMMA compared to the dispersions prepared in acetone. By Raman analysis, it is observed that the PMMA has no doping effect on the flakes. Composites with ABS are prepared with the obtained exfoliated flakes, attaining an enhancement in both the Young's modulus (≈22%) and tensile strength (≈17%) by using only 0.01 wt.% of filler loading. The oxygen permeability was also tested, showing an improvement in the gas barrier properties of the composite material, as the oxygen permeability is reduced of approximately 20% with 0.1 wt.% of FLG loading. In future, the effect of PMMA on the exfoliation of other two-dimensional crystals, such as hBN, MoS_2, and so on, and their use in polymer composites will be studied.

Experimental Section

Materials

Natural graphite flakes (+100 mesh) and acetone (ACS reagent, ≥99.5%) are purchased from Merck, poly(methyl methacrylate) powder (PMMA, molecular weight 550000) from Alfa Aesar, acrylonitrile butadiene styrene pellets (ABS, Terluran® GP22) from Ineos Styrosolution. All the materials are used without purification.

Production of the exfoliated graphite dispersions

Exfoliation of graphite: Two graphite dispersions are prepared, i) graphite (0.5 g) dispersed in acetone (0.05 L) and ii) in an acetone-PMMA mixture (0.05 L) containing 1 wt.% of PMMA with respect to acetone, in a glass vial. Graphite flakes are then exfoliated using an ultrasonic bath (VWR-Ultrasonic cleaner USC-THD) for 6 hours at a temperature ranging between 25 and 35 °C. The exfoliated graphite and PMMA dispersions in acetone are labelled "FLG-PMMA", while the dispersions produced in bare acetone are named "FLG".

Purification of the exfoliated graphite dispersions: We choose three centrifugal accelerations, that is, ≈200 *g* (gravitational acceleration corresponding to 1000 rpm for the rotor used), 4300 *g* (5000 rpm) and 17000 *g* (10000 rpm) for 30 minutes. The SBS is performed using a Beckman Coulter Optima XE-90 Ultracentrifuge (SW32Ti rotor). The 80% of the supernatant is collected after the centrifugation, while the precipitate is discarded.

Vacuum filtration: The concentration of the dispersions is measured through vacuum filtration, using polytetrafluoroethylene (PTFE) filters with a pore size of 0.2 μm (Merck Millipore). The mass of the filter is measured before ($M_{initial}$) and after (M_{final}) the vacuum filtration of a known volume (V_G) of the exfoliated graphite dispersion. The concentration is calculated by using Equation (3).

$$C = \frac{M_{initial} - M_{final}}{V_G} \quad (3)$$

In order to avoid the moisture weight and the acetone in M_{final}, the filters are dried before and after the filtration in a vacuum oven (Binder VLD 115) for 24 hours at 40 °C. Moreover, after the filtration of the dispersions FLG-PMMA centrifuged at 200, 4300 and 17000 *g*, the filters are washed with 50, 100 and 150 mL of acetone, respectively, so that the presence of PMMA does not affect the concentration.

Production of acrylonitrile butadiene styrene-exfoliated graphite composites

Six different ABS composites are prepared by using the solution blending method with different exfoliated graphite loadings with respect to ABS, ranging from 0.005 to 0.1 wt.%. The composites are prepared by using both FLG and FLG-PMMA dispersions. An ABS dispersion in acetone (30 wt.% of ABS) is prepared and mixed with both the FLG and FLG-PMMA dispersions and cast into glass petri dishes (diameter = 7.5 cm). Firstly, the films are dried in air (16 hours) and then in a vacuum oven (Binder VLD 115) at 30 °C (16 hours). Finally, the films are prepared by compression molding (Specac-Atlas Auto T8) by applying one metric ton of load at 180 °C. The thickness of the films is measured by using a caliper (Mahr 16EX) and it is about 200 μm.

Similarly, control samples are prepared containing the same amount of PMMA present in the FLG-PMMA and ABS composites, that is, 0.34, 0.68, 3.4 and 6.8 wt.% of PMMA with respect to ABS. The amount of PMMA used in the control samples corresponds to the same quantity present in the ABS-FLG-PMMA composites, e.g., the volume of FLG-PMMA dispersion used to prepare the composites having 0.05 wt.% of filler, contains 3.4 wt.% of PMMA. The prepared ABS dispersions (30 wt.%) are mixed with the acetone PMMA solution (1 wt.%), mixed using a sonic bath (VWR-Ultrasonic cleaner USC-THD) for 1 hour at a temperature ranging between 25–35 °C. The obtained mixtures are cast into the petri dishes. The acetone is removed by evaporation at room temperature overnight. Subsequently, the films are dried in a vacuum oven (Binder VLD 115) for 16 hours at 30 °C. Finally, the dried films are compression molded (Specac-Atlas Auto T8) applying 1 Ton of load at a

temperature of 180 °C, obtained a sample of ≈200 μm in thickness. The thickness of the film is measured with a calliper (Mahr 16EX).

Characterization

Characterization of the exfoliated graphite dispersions

Concentration of the exfoliated graphite dispersions: To confirm the concentration of exfoliated graphite flakes in the FLG-PMMA dispersions found through the vacuum filtration method, TGA and optical extinction spectroscopy are carried out on the FLG-PMMA sample centrifuged at 200 *g*.

Thermogravimetric analysis: The TGA analysis is carried out using a TGA Q500-TA Instrument in nitrogen atmosphere at a flow rate of 50 mL min^{-1}. Five samples are prepared by casting 1 mL of dispersion in the TGA Palladium pan. The analysis starts with an isothermal at 60 °C for 15 minutes to remove the solvent. Then, the temperature is decreased at 30 °C, followed by a heating ramp of 10 °C min^{-1} up to 800 °C.

Optical extinction spectroscopy (OES): Optical extinction spectroscopy is carried out in a Cary Varian 5000UV-Vis spectrophotometer. The *C* are evaluated using the optical extinction coefficient at 660 nm, using the Lambert law $A = \alpha lC$ in which *l* [m] is the light path length and α [L g^{-1} m^{-1}] is the extinction coefficient. Four samples are analyzed for each FLG-PMMA dispersion.

Viscosity and density measurements: The viscosity of acetone and the mixture acetone-1 wt.% PMMA is measured with a Discovery HR-2 Hybrid Rheometer (TA instruments), using a double-wall concentric cylinder geometry (inner diameter of 32 mm and outer diameter of 35 mm), designed for low-viscosity fluids. The shear rate is set at 50 s^{-1} with a temperature of 25 °C throughout all the measurements, three for each sample. The density is measured by weighing the mass of 1 mL of acetone and 1 mL of the mixture acetone-1 wt.% PMMA. The measure is repeated three times for each sample.

Contact angle: The surface tension measurements are performed with a Dataphysics OCAH200 contact angle goniometer equipped with a 2/300 CCD Chip camera at laboratory conditions (temperature 22–25 °C and relative humidity 50–60%). The surface tension is evaluated through the pendant drop method dispensing 12 μL of the different solutions at ambient temperature.[130,131] Moreover, the Young-Laplace equation is used for the calculations of the surface tension.[130,131]

Atomic force microscopy: The FLG-PMMA dispersions are filtered through vacuum filtration and washed with acetone. Then, the filters are sonicated for 30 minutes, re-dispersing the FLG flakes in acetone. The obtained dispersions are diluted 1:30 in acetone and 10 μL of the diluted dispersions are drop-cast onto Si/SiO_2 wafers and dried at 60 °C for 24 hours in a vacuum oven. AFM images are acquired with Bruker Innova AFM in tapping mode using silicon probes (frequency = 300 kHz, spring constant = 40 N m^{-1}). The thickness of 100 flakes is measured from the AFM images to perform the thickness statistics. Statistical analyses are fitted with log-normal distributions. *Analysis of PMMA traces by TGA:* The presence of PMMA residues on the AFM samples of the FLG-PMMA dispersion centrifuged at 200 *g* is evaluated using TGA. The FLG-PMMA dispersion rinsed from PMMA is deposited on the pan for an analysis and followed the same protocol used for the determination of concentration.

Transmission electron microscopy: The diluted exfoliated graphite dispersions are drop-cast onto TEM grids (Ultrathin C film on holey carbon on copper support film 400 mesh from Ted Pella Inc.). The TEM images and selected area electron diffraction (SAED) patterns are acquired in a Jeol JEM 1101 and the lateral sizes are measured using the software ImageJ. The lateral size statistics are performed on ≈100 flakes and fitted with log-normal distributions.

Raman spectroscopy: Raman measurements are carried out by means of a Renishaw inVia confocal Raman microscope using an excitation line of 514.5 nm (2.41 eV) with a 100× objective lens, and an incident power of 1 mW on the samples. Lorentzian functions are used to fit the peaks and 15 spectra are collected for each sample. The as-prepared exfoliated graphite dispersions are drop-cast onto a Si/SiO_2 wafer (LDB Technologies Ltd.) and dried under vacuum.

Characterization of acrylonitrile butadiene styrene-exfoliated graphite composites

Tensile testing: The tensile tests are carried out on dog-bone shaped specimens obtained from the compression moulded films. Fifteen specimens are tested for each composite. The specimen dimensions are chosen according to ASTM D882 Standard Test Methods for tensile properties of thin plastic sheeting. The tensile tests are performed using an Instron Dual Column Tabletop Universal Testing System 3365, with 3 mm min^{-1} cross-head speed.

Gas barrier measurements: The oxygen permeation tests of the as-prepared samples are performed using an Oxysense 5250i device (Oxysense, USA) equipped with a film permeation chamber. This machine is operated according to ASTM Method F3136-15 (ASTM 1989). The test is performed under the standard laboratory conditions, i.e., 23 °C and 50% relative humidity. The compression-moulded films are cut into a square piece (6×6 cm) and then placed inside the chamber. The OxySense fibre optic pen measures the oxygen reading from the oxydot, at specific time intervals. The oxygen transmission rate (OTR) of each film is measured by monitoring the oxygen uptake with time. Oxysense OTR software used this oxygen evolution to determine the OTR of films. Ten readings are taken for each sample with a minimum coefficient of determination (R^2) value of 0.995. The oxygen permeability, OP, of the films is then calculated according to Equation (4):

$$OP = \frac{OTRF_t}{\Delta p} \quad (4)$$

in which, OP is the oxygen permeability, OTR is the oxygen transmission rate, F_t is the film thickness, and Δp is the oxygen partial pressure.[132]

Acknowledgements

The authors acknowledge the financial support from the European Union's Horizon 2020 research and innovation program under grant agreement 785219-GrapheneCore2. S.G. also thanks the Educational Fund (Italy) for a Ph.D. scholarship. Moreover, the authors thank Giammarino Pugliese from the Nanochemistry laboratory of the Istituto Italiano di Tecnologia (IIT) for the thermogravimetric analysis, Riccardo Carzino from the Smart Materials laboratory of Istituto Italiano di Tecnologia (IIT) for the contact angle measurements, Uttam Paul from the Smart Materials laboratory of Istituto Italiano di Tecnologia (IIT) for the oxygen permeability measurements.

Conflict of interest

The authors declare no conflict of interest.

Keywords: 2D materials · graphene · liquid-phase exfoliation · polymer composites

[1] H. Jang, Y. J. Park, X. Chen, T. Das, M. S. Kim, J. H. Ahn, *Adv. Mater.* **2016**, *28*, 4184 – 4202.
[2] K. S. Kim, Y. Zhao, H. Jang, S. Y. Lee, J. M. Kim, K. S. Kim, J. H. Ahn, P. Kim, J. Y. Choi, B. H. Hong, *Nature* **2009**, *457*, 706 – 710.
[3] E. Torres Alonso, D. P. Rodrigues, M. Khetani, D.-W. Shin, A. De Sanctis, H. Joulie, I. De Schrijver, A. Baldycheva, H. Alves, A. I. S. Neves, S. Russo, M. F. Craciun, *npj Flex. Electron.* **2018**, *2*, 25.
[4] F. Schwierz, *Nat. Nanotechnol.* **2010**, *5*, 487 – 496.
[5] G. Fiori, F. Bonaccorso, G. Iannaccone, T. Palacios, D. Neumaier, A. Seabaugh, S. K. Banerjee, L. Colombo, *Nat. Nanotechnol.* **2014**, *9*, 768 – 779.
[6] G. Iannaccone, F. Bonaccorso, L. Colombo, G. Fiori, *Nat. Nanotechnol.* **2018**, *13*, 183 – 191.
[7] A. Scidà, S. Haque, E. Treossi, A. Robinson, S. Smerzi, S. Ravesi, S. Borini, V. Palermo, *Mater. Today* **2018**, *21*, 223 – 230.
[8] M. Romagnoli, V. Sorianello, M. Midrio, F. H. L. Koppens, C. Huyghebaert, D. Neumaier, P. Galli, W. Templ, A. D'Errico, A. C. Ferrari, *Nat. Rev. Mater.* **2018**, *3*, 392 – 414.
[9] A. Agresti, S. Pescetelli, B. Taheri, A. E. Del Rio Castillo, L. Cinà, F. Bonaccorso, A. Di Carlo, *ChemSusChem* **2016**, *9*, 2609 – 2619.
[10] F. Bonaccorso, Z. Sun, T. Hasan, A. C. Ferrari, *Nat. Photonics* **2010**, *4*, 611 – 622.
[11] F. Bonaccorso, L. Colombo, G. Yu, M. Stoller, V. Tozzini, A. C. Ferrari, R. S. Ruoff, V. Pellegrini, *Science* **2015**, *347*, 1246501.
[12] X. Li, L. Zhi, *Chem. Soc. Rev.* **2018**, *47*, 3189 – 3216.
[13] E. Pomerantseva, F. Bonaccorso, F. Feng, Y. Cui, Y. Gogotsi, *Science* **2019**, *366*, eaan8285.
[14] Y. Sun, G. Shi, *J. Polym. Sci. Part B* **2013**, *51*, 231 – 253.
[15] M. Miculescu, V. K. Thakur, F. Miculescu, S. I. Voicu, *Polym. Adv. Technol.* **2016**, *27*, 844 – 859.
[16] S. Stankovich, D. A. Dikin, G. H. B. Dommett, K. M. Kohlhaas, E. J. Zimney, E. A. Stach, R. D. Piner, S. B. T. Nguyen, R. S. Ruoff, *Nature* **2006**, *442*, 282 – 286.
[17] W. Chen, P. Xiao, H. Chen, H. Zhang, Q. Zhang, Y. Chen, *Adv. Mater.* **2019**, *31*, 1802403.
[18] S. Chatterjee, F. A. Nüesch, B. T. T. Chu, *Nanotechnology* **2011**, *22*, 275714.
[19] T. Hasan, Z. Sun, F. Wang, F. Bonaccorso, P. H. Tan, A. G. Rozhin, A. C. Ferrari, *Adv. Mater.* **2009**, *21*, 3874 – 3899.
[20] A. E. Del Rio Castillo, V. Pellegrini, A. Ansaldo, F. Ricciardella, H. Sun, L. Marasco, J. Buha, Z. Dang, L. Gagliani, E. Lago, N. Curreli, S. Gentiluomo, F. Palazon, P. Toth, E. Mantero, M. Crugliano, A. Gamucci, A. Tomadin, M. Polini, F. Bonaccorso, *Mater. Horiz.* **2018**, *5*, 890 – 904.
[21] K. R. Paton, E. Varrla, C. Backes, R. J. Smith, U. Khan, A. O'Neill, C. Boland, M. Lotya, O. M. Istrate, P. King, T. Higgins, S. Barwich, P. May, P. Puczkarski, I. Ahmed, M. Moebius, H. Pettersson, E. Long, J. Coelho, S. E. O'Brien, E. K. McGuire, B. M. Sanchez, G. S. Duesberg, N. McEvoy, T. J. Pennycook, C. Downing, A. Crossley, V. Nicolosi, J. N. Coleman, *Nat. Mater.* **2014**, *13*, 624 – 630.
[22] A. C. Ferrari, F. Bonaccorso, V. Fal'ko, K. S. Novoselov, S. Roche, P. Bøggild, S. Borini, F. H. L. Koppens, V. Palermo, N. Pugno, J. A. Garrido, R. Sordan, A. Bianco, L. Ballerini, M. Prato, E. Lidorikis, J. Kivioja, C. Marinelli, T. Ryhänen, A. Morpurgo, J. N. Coleman, V. Nicolosi, L. Colombo, A. Fert, M. Garcia-Hernandez, A. Bachtold, G. F. Schneider, F. Guinea, C. Dekker, M. Barbone, Z. Sun, C. Galiotis, A. N. Grigorenko, G. Konstantatos, A. Kis, M. Katsnelson, L. Vandersypen, A. Loiseau, V. Morandi, D. Neumaier, E. Treossi, V. Pellegrini, M. Polini, A. Tredicucci, G. M. Williams, B. Hee Hong, J.-H. Ahn, J. Min Kim, H. Zirath, B. J. van Wees, H. van der Zant, L. Occhipinti, A. Di Matteo, I. A. Kinloch, T. Seyller, E. Quesnel, X. Feng, K. Teo, N. Rupesinghe, P. Hakonen, S. R. T. Neil, Q. Tannock, T. Löfwander, J. Kinaret, *Nanoscale* **2015**, *7*, 4598 – 4810.
[23] F. Bonaccorso, A. Lombardo, T. Hasan, Z. Sun, L. Colombo, A. C. Ferrari, *Mater. Today* **2012**, *15*, 564 – 589.
[24] M. I. Kairi, M. Khavarian, S. A. Bakar, B. Vigolo, A. R. Mohamed, *J. Mater. Sci.* **2018**, *53*, 851 – 879.
[25] N. Lisi, T. Dikonimos, F. Buonocore, M. Pittori, R. Mazzaro, R. Rizzoli, S. Marras, A. Capasso, *Sci. Rep.* **2017**, *7*, 9927.
[26] D. Luo, M. Wang, Y. Li, C. Kim, K. M. Yu, Y. Kim, H. Han, M. Biswal, M. Huang, Y. Kwon, M. Goo, D. C. Camacho-Mojica, H. Shi, W. J. Yoo, M. S. Altman, H. J. Shin, R. S. Ruoff, *Adv. Mater.* **2019**, *31*, 1903615.
[27] X. Li, W. Cai, J. An, S. Kim, J. Nah, D. Yang, R. Piner, A. Velamakanni, I. Jung, E. Tutuc, S. K. Banerjee, L. Colombo, R. S. Ruoff, *Science* **2009**, *324*, 1312 – 1314.
[28] N. Mishra, J. Boeckl, N. Motta, F. Iacopi, *Phys. Status Solidi A* **2016**, *213*, 2277 – 2289.
[29] M. Beshkova, L. Hultman, R. Yakimova, *Vacuum* **2016**, *128*, 186 – 197.
[30] W. A. De Heer, C. Berger, M. Ruan, M. Sprinkle, X. Li, Y. Hu, B. Zhang, J. Hankinson, E. Conrad, *Proc. Natl. Acad. Sci. USA* **2011**, *108*, 16900 – 16905.
[31] K. V. Emtsev, A. Bostwick, K. Horn, J. Jobst, G. L. Kellogg, L. Ley, J. L. McChesney, T. Ohta, S. A. Reshanov, J. Röhrl, E. Rotenberg, A. K. Schmid, D. Waldmann, H. B. Weber, T. Seyller, *Nat. Mater.* **2009**, *8*, 203 – 207.
[32] C. Berger, Z. Song, T. Li, X. Li, A. Y. Ogbazghi, R. Feng, Z. Dai, A. N. Marchenkov, E. H. Conrad, P. N. First, W. A. De Heer, *J. Phys. Chem. B* **2004**, *108*, 19912 – 19916.
[33] K. S. Novoselov, D. Jiang, F. Schedin, T. J. Booth, V. V. Khotkevich, S. V. Morozov, A. K. Geim, *Proc. Natl. Acad. Sci. USA* **2005**, *102*, 10451 – 10453.
[34] X. Lu, M. Yu, H. Huang, R. S. Ruoff, *Nanotechnology* **1999**, *10*, 269 – 272.
[35] Y. Hernandez, V. Nicolosi, M. Lotya, F. M. Blighe, Z. Sun, S. De, I. T. McGovern, B. Holland, M. Byrne, Y. K. Gun'Ko, J. J. Boland, P. Niraj, G. Duesberg, S. Krishnamurthy, R. Goodhue, J. Hutchison, V. Scardaci, A. C. Ferrari, J. N. Coleman, *Nat. Nanotechnol.* **2008**, *3*, 563 – 568.
[36] J. N. Coleman, M. Lotya, A. O'Neill, S. D. Bergin, P. J. King, U. Khan, K. Young, A. Gaucher, S. De, R. J. Smith, I. V. Shvets, S. K. Arora, G. Stanton, H.-Y. Kim, K. Lee, G. T. Kim, G. S. Duesberg, T. Hallam, J. J. Boland, J. J. Wang, J. F. Donegan, J. C. Grunlan, G. Moriarty, A. Shmeliov, R. J. Nicholls, J. M. Perkins, E. M. Grieveson, K. Theuwissen, D. W. McComb, P. D. Nellist, V. Nicolosi, *Science* **2011**, *331*, 568 – 571.
[37] J. S. Bunch, Y. Yaish, M. Brink, P. Bolotin, P. L. Mc Euen, *Nano Lett.* **2005**, *5*, 287 – 290.
[38] A. Ciesielski, P. Samorì, *Chem. Soc. Rev.* **2014**, *43*, 381 – 398.
[39] S. Yang, M. R. Lohe, K. Müllen, X. Feng, *Adv. Mater.* **2016**, *28*, 6213 – 6221.
[40] A. A. Green, M. C. Hersam, *Nano Lett.* **2009**, *9*, 4031 – 4036.
[41] A. Liscio, K. Kouroupis-Agalou, X. Diez Betriu, A. Kovtun, E. Treossi, N. M. Pugno, G. De Luca, L. Giorgini, V. Palermo, *2D Mater.* **2017**, *4*, 025017.
[42] Z. Wang, S. Wu, J. Zhang, P. Chen, G. Yang, X. Zhou, Q. Zhang, Q. Yan, H. Zhang, *Nanoscale Res. Lett.* **2012**, *7*, 161.
[43] J. N. Israelachvili, *Intermolecular and Surface Forces*, Academic Press, Amsterdam, **2015**.
[44] A. E. Del Rio Castillo, M. Cesar, E. Diez-Barra, E. Vázquez, *Nano Res.* **2014**, *7*, 963 – 972.
[45] F. Bonaccorso, A. Bartolotta, J. N. Coleman, C. Backes, *Adv. Mater.* **2016**, *28*, 6136 – 6166.
[46] J. Lyklema, *Colloids Surf. A* **1999**, *156*, 413 – 421.
[47] H. M. Solomon, B. A. Burgess, G. L. Kennedy, R. E. Staples, B. A. Burgess, G. L. Kennedy, R. E. Staples, *Drug Chem. Toxicol.* **1995**, *18*, 271 – 293.
[48] L. Schep, K. Knudsen, R. Slaughter, J. Vale, B. Mégarbane, *Clin Toxicol* **2012**, *50*, 458 – 470.
[49] D. R. Lide, *CRC Handbook of Chemistry and Physics*, CRC Press, Boca Raton, **2004**.
[50] P. K. Mallick, *Processing of Polymer Matrix Composites: Processing and Applications*, CRC Press, Boca Raton, **2017**.
[51] S. X. Zheng, *Principles of Organic Coatings and Finishing*, Cambridge Scholars Publishing, Newcastle, **2019**.
[52] T. Hasan, P. H. Tan, F. Bonaccorso, A. G. Rozhin, V. Scardaci, W. I. Milne, A. C. Ferrari, *J. Phys. Chem. C* **2008**, *112*, 20227 – 20232.
[53] P. K. Mallick, *Fiber-Reinforced Composites: Materials, Manufacturing, and Design, 2nd Ed.*, CRC Press, Boca Raton, **1993**.
[54] M. Berber, H. H. Inas, *Carbon Nanotubes: Current Progress of Their Polymer Composites*, London, **2016**.

[55] E. Jiménez, B. Cabañas, G. Lefebvre, *Environment, Energy and Climate Change I: Environmental Chemistry of Pollutants and Wastes*, Springer, Cham, **2015**.
[56] G. Rabilloud, *High-Performance Polymers: Chemistry and Applications*, Editions Technip, Paris, **1997**.
[57] J. D Christesen, B.Sc. Thesis, *Mechanical Properties of Solvent Cast Graphene- Polymer Nanocomposites*, **2011**.
[58] A. G. D'Aloia, A. Proietti, H. C. Bidsorkhi, A. Tamburrano, G. De Bellis, F. Marra, A. Bregnocchi, M. S. Sarto, *Polymers* **2018**, *10*, 82.
[59] T. Carey, S. Cacovich, G. Divitini, J. Ren, A. Mansouri, J. M. Kim, C. Wang, C. Ducati, R. Sordan, F. Torrisi, *Nat. Commun.* **2017**, *8*, 1202.
[60] A. Capasso, A. E. Del Rio Castillo, H. Sun, A. Ansaldo, V. Pellegrini, F. Bonaccorso, *Solid State Commun.* **2015**, *224*, 53 – 63.
[61] J. Baker, D. Deganello, D. T. Gethin, T. M. Watson, *Mater. Res. Innovations* **2014**, *18*, 86 – 90.
[62] V. H. Pham, T. V. Cuong, S. H. Hur, E. W. Shin, J. S. Kim, J. S. Chung, E. J. Kim, *Carbon* **2010**, *48*, 1945 – 1951.
[63] F. Yener, O. Jirsak, R. Gemci, *Iran. J. Chem. Chem. Eng.* **2012**, *31*, 49 – 58.
[64] Y. T. Liang, M. C. Hersam, *J. Am. Chem. Soc.* **2010**, *132*, 17661 – 17663.
[65] A. S. Wajid, S. Das, F. Irin, H. S. T. Ahmed, J. L. Shelburne, D. Parviz, R. J. Fullerton, A. F. Jankowski, R. C. Hedden, M. J. Green, *Carbon* **2012**, *50*, 2065.
[66] U.S. Environmental Protection Agency, *Toxicological Review of Acetone*, EPA, **2001**.
[67] M. Crabbe-Mann, D. Tsaoulidis, M. Parhizkar, M. Edirisinghe, *Cellulose* **2018**, *25*, 1687 – 1703.
[68] A. Arostegui, M. Sarrionandia, J. Aurrekoetxea, I. Urrutibeascoa, *Polym. Degrad. Stab.* **2006**, *91*, 2768 – 2774.
[69] P. Slobodian, A. Lenganova, P. Saha, M. Slouf, *J. Reinf. Plast. Compos.* **2007**, *26*, 1705 – 1712.
[70] A. E. Del Río Castillo, C. D. Reyes-Vazquez, L. E. Rojas-Martinez, V. Pellegrini, F. Bonaccorso, *FlatChem* **2019**, *18*, 100131.
[71] J. Xie, H. Ye, Q. Zhang, L. Li, M. Jiang, *Polym. Int.* **1997**, *44*, 35 – 40.
[72] S. Sankaranarayanan, J. Hermosilla, F. Acevedo, R. Navia, *Compos. Commun.* **2018**, *10*, 18 – 24.
[73] A. V. Puga, R. Garcia-Valls, S. Fernández-Prieto, J. Smets, D. York, *J. Appl. Polym. Sci.* **2014**, *131*, 40870.
[74] S. Yano, K. Nakamura, M. Kodomari, N. Yamauchi, *J. Appl. Polym. Sci.* **1994**, *54*, 163 – 176.
[75] J. J. Jasper, *J. Phys. Chem. Ref. Data* **1972**, *1*, 841 – 1010.
[76] A. O'Neill, U. Khan, P. N. Nirmalraj, J. Boland, J. N. Coleman, *J. Phys. Chem. C* **2011**, *115*, 5422 – 5428.
[77] P. May, U. Khan, J. M. Hughes, J. N. Coleman, *J. Phys. Chem. C* **2012**, *116*, 11393 – 11400.
[78] M. T. Popescu, D. Tasis, K. D. Papadimitriou, S. Gkermpoura, C. Galiotis, C. Tsitsilianis, *RSC Adv.* **2015**, *5*, 89447 – 89460.
[79] Arkema, http://arkema.com.
[80] D. G. Poitout, *Biomechanics and Biomaterials in Orthopedics*, Springer, London, **2016**.
[81] A. Paydayesh, A. Arefazar, A. Jalaliarani, *J. Appl. Polym. Sci.* **2016**, *133*, 1 – 12.
[82] S. K. Swain, G. Prusty, A. S. Ray, L. Behera, *J. Exp. Nanosci.* **2014**, *9*, 240 – 248.
[83] S. Mohamadi, N. Sharifi-sanjani, A. Foyouhi, *J. Polym. Res.* **2013**, *20*, 46.
[84] N. Belhaneche-Bensemra, *Macromol. Symp.* **2002**, *180*, 203 – 215.
[85] M. M. Abutalib, *Physica B* **2019**, *552*, 19 – 29.
[86] S. Jabeen, S. Gul, A. Kausar, B. Muhammad, F. Muhammad, *Polym. Plast. Technol. Eng.* **2018**, *58*, 427 – 442.
[87] I. A. Disher Al-Hydary, L. M. Manocha, P. M. George, *IQJMME* **2012**, *12*, 709 – 722.
[88] A. C. Ferrari, J. C. Meyer, V. Scardaci, C. Casiraghi, M. Lazzeri, F. Mauri, S. Piscanec, D. Jiang, K. S. Novoselov, S. Roth, A. K. Geim, *Phys. Rev. Lett.* **2006**, *97*, 187401.
[89] A. C. Ferrari, D. M. Basko, *Nat. Nanotechnol.* **2013**, *8*, 235 – 246.
[90] F. Bonaccorso, P.-H. Tan, A. C. Ferrari, *ACS Nano* **2013**, *7*, 1838 – 1844.
[91] A. Das, B. Chakraborty, A. K. Sood, *Bull. Mater. Sci.* **2008**, *31*, 579 – 584.
[92] L. Liu, M. Qing, Y. Wang, S. Chen, *J. Mater. Sci. Technol.* **2015**, *31*, 599 – 606.
[93] A. Rajabpour, S. Kimiagar, F. Tavazoee, *Phys. Chem. Res.* **2015**, *3*, 299 – 304.
[94] N. Jing, Q. Xue, C. Ling, M. Shan, T. Zhang, X. Zhou, Z. Jiao, *RSC Adv.* **2012**, *2*, 9124 – 9129.
[95] M. V. Bracamonte, G. I. Lacconi, S. E. Urreta, L. E. F. F. Torres, *J. Phys. Chem. C* **2014**, *118*, 15455 – 15459.
[96] A. Paydayesh, A. Arefazar, A. Jalaliarani, *J. Appl. Polym. Sci.* **2016**, *133*, 43799.
[97] R. J. Smith, M. Lotya, J. N. Coleman, *New J. Phys.* **2010**, *12*, 125008 – 125019.
[98] P. Lin, J. Wu, W. Liu, *Sci. Rep.* **2018**, *8*, 9766.
[99] A. Reina, X. Jia, J. Ho, D. Nezich, H. Son, V. Bulovic, M. S. Dresselhaus, K. Jing, *Nano Lett.* **2009**, *9*, 30 – 35.
[100] A. Gupta, G. Chen, P. Joshi, S. Tadigadapa, P. C. Eklund, *Nano Lett.* **2006**, *6*, 2667 – 2673.
[101] L. Graphene, Y. K. Koh, M. Bae, D. G. Cahill, E. Pop, *ACS Nano* **2011**, *5*, 269 – 274.
[102] E. Bordes, B. Morcos, D. Bourgogne, J. M. Andanson, P. O. Bussière, C. C. Santini, A. Benayad, M. C. Gomes, A. A. H. Pádua, *Front. Chem.* **2019**, *7*, 223.
[103] W. Zhao, B. Xia, L. Lin, X. Xiao, P. Liu, X. Lin, H. Peng, Y. Zhu, R. Yu, P. Lei, J. Wang, L. Zhang, Y. Xu, M. Zhao, L. Peng, Q. Li, W. Duan, Z. Liu, S. Fan, K. Jiang, *Sci. Adv.* **2017**, *3*, e1603231.
[104] Q. Wan, H. Wang, S. Li, J. Wang, *J. Colloid Interface Sci.* **2018**, *526*, 167 – 173.
[105] O. M. Maragó, F. Bonaccorso, R. Saija, G. Privitera, P. G. Gucciardi, M. A. Iatì, G. Calogero, P. H. Jones, F. Borghese, P. Denti, V. Nicolosi, A. C. Ferrari, *ACS Nano* **2010**, *4*, 7515 – 7523.
[106] E. G. Pickels, *J. Gen. Physiol.* **1943**, *26*, 341.
[107] P. K. O. Svedberg, *The Ultracentrifuge*, Clarendon Press, Oxford, **1940**.
[108] G. Kakavelakis, A. E. Del Rio Castillo, V. Pellegrini, A. Ansaldo, P. Tzourmpakis, R. Brescia, M. Prato, E. Stratakis, E. Kymakis, F. Bonaccorso, *ACS Nano* **2017**, *11*, 3517 – 3531.
[109] A. E. Del Rio Castillo, V. Pellegrini, H. Sun, J. Buha, D. A. Dinh, E. Lago, A. Ansaldo, A. Capasso, L. Manna, F. Bonaccorso, *Chem. Mater.* **2018**, *30*, 506 – 516.
[110] H. Sun, A. Varzi, V. Pellegrini, D. A. Dinh, R. Raccichini, A. E. Del Rio Castillo, *Solid State Commun.* **2017**, *251*, 88 – 93.
[111] H. Sanaeepur, A. Ebadi Amooghin, A. Moghadassi, A. Kargari, S. Moradi, D. Ghanbari, *Polym. Adv. Technol.* **2012**, *23*, 1207 – 1218.
[112] J. Y. Shur, B. Ranby, *J. Appl. Polym. Sci.* **1976**, *20*, 3121 – 3131.
[113] H. Sanaeepur, A. E. Amooghin, A. Moghadassi, A. Kargari, *Sep. Purif. Technol.* **2011**, *80*, 499 – 508.
[114] G. Shi, S. Araby, C. T. Gibson, Q. Meng, S. Zhu, J. Ma, *Adv. Funct. Mater.* **2018**, *28*, 1706705.
[115] B. K. Kim, *J. Appl. Polym. Sci.* **1993**, *47*, 1581 – 1587.
[116] J. A. Pathak, R. H. Colby, S. Y. Kamath, S. K. Kumar, R. Stadler, *Macromolecules* **1998**, *31*, 8988 – 8997.
[117] G. N. Kumaraswamy, C. Ranganathaiah, M. V. Deepa Urs, H. B. Ravikumar, *Eur. Polym. J.* **2006**, *42*, 2655 – 2666.
[118] N. T. Qazvini, E. Chehrazi, *J. Macromol. Sci. Part B* **2011**, *50*, 2165 – 2177.
[119] K. Naito, G. E. Johnson, D. L. Allara, T. K. Kwei, *Macromolecules* **1978**, *11*, 1260 – 1265.
[120] J. R. Davis, *Tensile Testing, 2nd Ed.*, ASM International, Materials Park, **2004**.
[121] Q. Waheed, A. N. Khan, R. Jan, *Polymer* **2016**, *97*, 496 – 503.
[122] S. Dul, L. Fambri, A. Pegoretti, *Composites Part A* **2016**, *85*, 181 – 191.
[123] S. Dul, A. Pegoretti, L. Fambri, *Nanomaterials* **2018**, *8*, 674.
[124] S. Dul, L. Fambri, C. Merlini, G. M. O. Barra, M. Bersani, L. Vanzetti, A. Pegoretti, *Polym. Compos.* **2019**, *40*, E285 – E300.
[125] S. N. Tripathi, G. S. S. Rao, A. B. Mathur, R. Jasra, *RSC Adv.* **2017**, *7*, 23615 – 23632.
[126] Y. Cui, S. I. Kundalwal, S. Kumar, *Carbon* **2016**, *98*, 313 – 333.
[127] T. V. Varghese, H. Ajith Kumar, S. Anitha, S. Ratheesh, R. S. Rajeev, V. Lakshmana Rao, *Carbon* **2013**, *61*, 476 – 486.
[128] K. J. Berean, J. Z. Ou, M. Nour, M. R. Field, M. M. Y. A. Alsaif, Y. Wang, R. Ramanathan, V. Bansal, S. Kentish, C. M. Doherty, A. J. Hill, C. McSweeney, R. B. Kaner, K. Kalantar-Zadeh, *J. Phys. Chem. C* **2015**, *119*, 13700 – 13712.

[129] S. Daradmare, S. Raj, A. R. Bhattacharyya, S. Parida, *Composites Part B* **2018**, *155*, 1 – 10.
[130] F. K. Hansen, G. Rødsrud, *J. Colloid Interface Sci.* **1991**, *141*, 1 – 9.
[131] J. D. Berry, M. J. Neeson, R. R. Dagastine, D. Y. C. Chan, R. F. Tabor, *J. Colloid Interface Sci.* **2015**, *454*, 226 – 237.
[132] H. Y. Hui, *Handbook of Food Science Technology and Engineering, Vol. 3*, CRC Press, Boca Raton, **2006**.

Manuscript received: February 1, 2020
Accepted manuscript online: March 26, 2020
Version of record online: April 17, 2020